DYNAMIC TENSILE FRACTURE PHENOMENA AT WAVE PROPAGATION IN CERAMIC BARS

JERZY NAJAR

Department A of Mechanics, University of Technology, Munich, Germany

1 Abstract

Spalling experiments with high performance ceramics performed in the uniaxial state of stress at room and elevated temperatures are discussed here from the point of view of the applicability of the one dimensional wave pattern in the framework of the continuum damage mechanics of brittle elastic materials. The testing apparatus is presented, and the details of the evaluation procedure for stresses in the propagating wave and at fracture are given. Attention is paid to the carefull analysis of the experimental data, in order to distinguish between geometrical and material wave dispersion phenomena as well as to account for the effects of inhomogeneity of the temperature field in the specimen. Effects of multiple spalling are analysed with the aim to distinguish between primary and secondary fractures, which results in proper assessment of the dynamic tensile strength of the ceramic material in dependence of the testing temperature.

1.1 Keywords

Dynamic strength, fracture, continuum damage, elevated temperature, multiple spalling, wave dispersion.

2 Introduction

The dominant mode of failure of high performance ceramics under dynamic loading is spalling. Compressive fracture phenomena in ceramics, when associated with shearing mechanisms, s. Horii at al, 1986, are generally activated at much higher levels of acting stress than tensile damage effects, s. Najar, 1987, even at static loading. This remains true in the dynamic case, at least at load wave lengths corresponding to frequencies below the resonance of the micro-sources of damage, i.e. practically at strain rates not higher than 10^3 s^{-1}, as well as at elevated temperatures enhancing splitting and shearing failure to the same extent. Therefore, in view of multiple applications of these materials in extreme thermal and dynamic situations, the determination of their dynamic tensile strength becomes an important task.

The most widely used apparatus for dynamic testing, the split Hopkinson pressure bar (SHPB), s. Davies, 1948, cannot be effectively applied at these experiments. The main reason is related to the fact that the evaluation procedure in the SHPB experiments is based upon the assumption of multiple reflections of the wave within the specimen, leading to quasi-static yielding, s. Kolsky, 1953. This hardly applies to the brittle failure of ceramics, where the spall develops within a single wave passage, provided the stress amplitude is sufficiently high. Also, the known tensile versions of the SHPB set-up, e.g. Nicholas, 1981, demand complicated geometries of the specimens and need to accommodate for gripping devices, a task difficult to fulfill with high performance ceramics.

On the other hand, the variety of Charpy-type tensile devices in use, e.g. Kussmaul et al., 1989, lack the advantage of operating with a non-instrumented specimen of a simple geometry, typical for the SHPB set-up. Therefore, complicated wave patterns dominate the field, which necessitates the use of extensive numerical calculations for the evaluation of the results. Moreover, testing of instrumented specimens in elevated temperatures is practically impossible with the strain gauges available at the time.

Finally, the plate impact arrangement, s. Barker et al., 1964, although superb for basic research of spalling phenomena, seems to be forbiddingly expensive, when a larger number of specimens need to be tested in order to overcome the handicap of the relatively high natural scatter of mechanical properties, typical for ceramics and like materials. Moreover, the material data on uniaxial strain response obtained in this apparatus need to be complemented with data on tensile response at dynamic uniaxial stress.

It was for all the reasons listed above as well as on the basis of the specific properties of ceramic materials, particularly their low fracture toughness, very short fracture delay time, s. Duffy et al., 1989, and high compressive - to - tensile strength ratio, that the experimental procedure presented in this paper has been developed.

3 Experimental arrangement

The testing device and evaluation method, conceived at the Department of Mechanics, Munich University of Technology, with the financial support of the German Research Community (DFG), combine the principles of the pulse initiation and its measurement, typical for the SHPB method, with the tensile dynamic loading of the specimen arising in result of the reflection of the compressive stress wave from its free end, characteristic for spalling experiments in uniaxial strain. However, the slenderness of the specimen, and a carefully chosen pulse profile result in the spalling effect developing sufficiently far away from the point of reflection to secure uniaxial stress, Fig. 1.

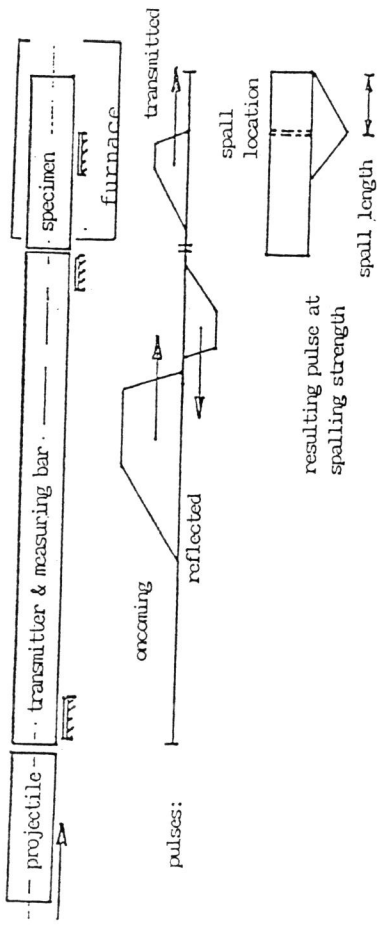

Figure 1: Experimental arrangement

The apparatus consists of a launcher (compressed air gun: barell 2.5 m, caliber 20.5 mm, driving pressure up to 30 atm, muzzle projectile speed up to more than 100 m/sek), lined up with the instrumented transmitter bar (slenderness ratio up to 100), which is co-axially placed next to the cylindrical specimen (slenderness ratio 20 and more). For experiments at elevated temperatures, the specimen can be placed in an open-end furnace oriented along the axis of the set-up. In this case, an extension piece of the same material as the specimen is positioned between the transmitter bar and the tested sample in order to bridge over the thermally inhomogeneous field at the opening of the funace. Finally, to prevent postsecondary fractures, a fragment trap is situated at the far end of the set-up.

The compressive pulse of the needed form is induced in the transmitter bar by the impact of a properly shaped projectile, with the impact speed corresponding to a stress amplitude σ_i within the elastic range of the bar.

As the pulse travels along the bar, it gets registered at the gauge station and stored in the oscilloscope. At the interface between the transmitter bar and the specimen a reflected pulse σ_r resulting from the difference of the effective impedances begins to travel back to the gauge, to get registered and stored. It is easy distinguishable from the pulse σ_i, when a favourable combination of its basic period and the travel time between the gauge and the bar end

has been selected.

A part of the compressive pulse, σ_t, gets transmitted into the specimen. It propagates in it without causing material damage, when the impedance ratio is correctly chosen, for the given pulse σ_i.

As it arrives at the free end, it gets reflected as a tensile pulse and superposed upon the still arriving tail of the pulse σ_t, s. Kolsky, 1953. The resulting stress distribution leads to tensile stresses increasing with the distance from the free end and growing in time, Fig. 2.

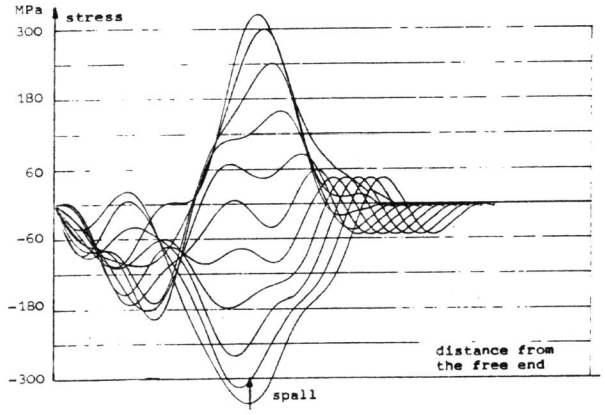

Figure 2: Resulting transient pulses in the specimen in a time-step sequence

As soon as the peak σ_{max} of the resulting stress distribution reaches the level of the dynamic tensile strength σ_{spall} of the material, spall takes place: a slender fragment splits from the end of the specimen and the momentum trapped in it detaches it from the specimen.

The knowledge of the site of the spall, the time of its occurence and the level of the resulting tensile stress at the place and at the instant of the fracture should determine the dynamic tensile strength.

4 Evaluation procedure

The evaluation procedure consists of four steps:

1. The uniaxial linear elastic approximation of the wavetrain.
2. The correction of the stress distributions for geometrical dispersive effects developing during propagation due to the dependence of the harmonic components' wave-speed on the ratio of the bar radius to its wavelength (Pochhammer - Chree effect).
3. The determination of the primary spalling site in case of multiple fracture.
4. The estimation of the influence of material non-linerity due to continuum damage in the tensile loading preceeding spalling fracture.

The first three steps of the evaluation procedure, as well as some experimental results based on the related modelling, are briefly presented in this chapter. The influence of damage-related non-linearity shall be discussed separately in Ch. 5. Additional aspects of the evaluation with regards to the experiments at elevated temperatures, handling therefore with problems of the wave propagation in non-homogeneous temperature fields, are discussed in a separate paper, Najar at al., 1993.

The basic assumptions of the evaluation procedure are related to the specific experimental configuration and the properties of the tested ceramics.

1. The slenderness of the transmitter bar and the specimen allows for applying the uniaxial stress wave model, with corrective terms for geometrical dispersive effects, s. Kolsky, 1953, for the best part of the sequence of the events. Also, when the distance of the spalling site from the free end of the specimen can be obtained sufficiently large, it results likewise in the formation of a uniaxial stress wave pattern.

2. The high ratio of the compressive-to-tensile strength typical for ceramics confines the damage and fracture phenomena to the very last stage of the process, and limits thus the non-linear material response to the short range between the free end and the spalling site.

3. The characteristically small fracture activation time in ceramics under sufficiently high tensile stress, Rajendran at al., 1988, allows in the present experiments, at the effective registration frequence of 1 MHz, to identify the peak stress σ_{max} with the strength. For additional aspects of the variable loading at non-linear response, s. Ch. 5.

4. The combination of the almost plane wavefront of the uniaxial pattern with the small fracture delay at high acting stress leads to a quasi-homogeneous damage evolution and fracture within most of the specimen's cross-sections, s. Bellendir at al., 1989.

To assure a unequivocal determination of the spalling strength it is necessary to induce in the transmitter bar a properly shaped pulse σ_i. Superposing it with the accordingly time-shifted pulse σ_r, introducing corrections for the geometrical dispersion and taking into account the effective impedances relation, Kolsky, 1953, one obtains numerically the transmitted pulse σ_t.

Its propagation within the specimen, as long as it remains compressive, corresponds further to the elastic rod wave pattern. Moreover, for most sorts of

ceramics, the tested specimens are thinner than the transmitter bar. Added to the twice higher wave speed in the ceramics than in steel this results in the shifting of the Fourier spectrum of the transmitted pulse towards the higher wavelength-to-radius ratio, which in turn means almost negligible dispersion effects in the specimen.

The next subroutine determines the reflection from the free end of the specimen and the superposition of the compressive and tensile transient waves. The resulting stress distributions in the specimen are then presented in a 0.5 μsec time-step sequence, Fig. 2.

The steady growth of the resulting tensile amplitude and the simultaneous steady drift of the position of the stress maximum, away from the free end of the specimen, result in an easy determination of the spalling stress σ_{spall} by setting it equal with the value of the stress peak σ_{max} at the instance of its spatial coincidence with the location of the spall found in the experiment. This yields at the same time the instance of the spalling.

In some tests, there is multiple spalling rather than single fracture observed. The question arises, how to distinguish here the primary spall from fractures secondary in time, provided no simultaneous spalling due to inhomogeneous strength distribution in the specimen takes place, Fig. 3. The latter case belongs to the usual statistical treatment of experimental series at randomly distributed strength properties of the material.

The case of subsequent spalling is more important for the evaluation procedure. We atribute the phenomenon to secondary reflections of the compressive pulse's wavetail arriving at the cross-section, where the spalling fracture has already occured: here, the superposition of the oncoming compressive stress train with the reflected tensile pulse takes place, analogous to that at the end of the specimen, leading again to spalling at some distance from the primary

spall.

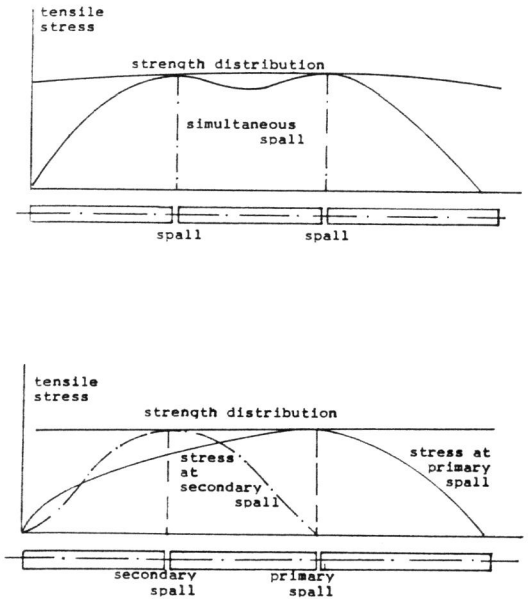

Figure 3: Multiple spall occurence: (a) simultaneous spall, (b) subsequent spall

Direct observations by means of high-speed photography or registration of breakage in the conducting coating of the specimen cannot provide easy answers, due to a disadvantageous ratio of the low fragment velocity to the high wave-speed (ca. 1:1000) in experiments with ceramics. At multiple fractures occuring at distances of about 20 mm from each other, Table 1, the delay of the subsequent spalls of less than 2 μsec would correspond to differences in

gaps between flying fragments of some 20 μm, a distance hardly measurable at uneven fracture surfaces at low costs.

An indirect method of determination of the location of the primary spall has been developed therefore, based on the tracing of the time sequence of the stress distributions over the length of the specimen, Fig. 4.

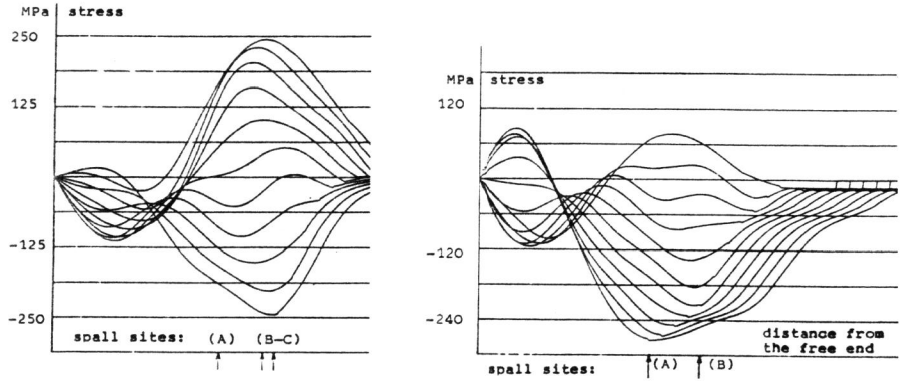

Figure 4: Time-step sequences leading to a multiple sequential spall: (a) monotonic stress peak path; (b) vaccillating stress peak path

For a given test, one compares the path of the tensile stress peak $\sigma_{max}(x,t)$ in the stress-to-distance plane with the experimentally determined spall locations. In most cases, when the resulting pulse has been favourably shaped, the path leads unequivocally towards one of the locations, not necessarily the one closest to the free end of the specimen, as it was originally believed, Fig. 4a. This location is thus considered to represent the primary spalling, and the corresponding peak stress equals to the dynamic tensile strength of the material.

In some cases, the peak path may vaccillate between two spall locations, Fig. 4b. Here, two aspects should be taken into account when looking for the primary site. First, it is with higher probability the location, which is approached by the peak path $\sigma_{max}(x)$ at stress values close to the dynamic tensile strength σ_{spall} determined in other experiments of the series. Secondly, one can extend the time-step sequence of stress distributions beyond the instance of spall, by analysing a simple cut-off procedure, which rejects the pulse tail trapped within one of the fragments, Fig. 5, and tracing the reflection of the remainder from the new free end at the hypothetic primary spall location.

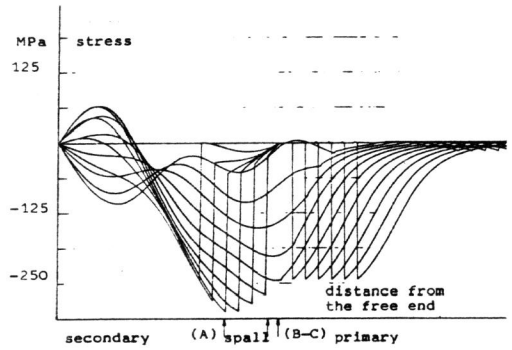

Figure 5: Cut-off time-step procedure for determination of the secondary spall

Even though the losses due to the fracture resistance energy in the primary spalling are thus not taken into account, the shifting of the post-spalling peak path shows the same tendency to move towards the secondary spall location,

confirming the initial hypothesis.

Table 1: Determination of the dynamic tensile strength of alumina rods at multiple spalling (distances measured from the free end of the specimen)

no.	spall locations mm	primary loc. mm	spall strength MPa	comments
1	61; 77-81	80.5	242	damage within 77-81 mm
2	102.5	102.5	287	no secondary spall
3	65; 81	65	271	
4	35; 87-90	87-90	289	indefinite location
5	58; 88; 97	88		registration failure
6				spall after many reflect.
7	37; 83; 109	83	226	
8				spall after many reflect.
9	26; 71	71	340	stress peak at 70 mm
10	71; 84; 106	71	281	
11	42; 66; 85; 105	66	295	
12	60; 79; 93	79	281	stress peak at 78 mm
13	56; 72; 95	72	225	stress peak at 71 mm

The resulting data for a room temperature test series with monolithic alumina rods are presented in Table 1. Observe that only in 3 out of 10 completed tests the primary spall site corresponds to the fracture at a location nearest to the free end of the specimen, as it was originally assumed, s. Bierwirth at al., 1990. The mean value of the dynamic tensile stress in the series, s. Table 1, equals 273 MPa, at the standard deviation of 35 MPa, which amounts to 12.8 % of the mean strength. Rejecting test nr. 9, as a clear stray shot, one

obtains correspondingly 266 MPa for the tensile strength at 10.4 % of the relative error.

Obviously, the sequential analysis of the stress distributions results in an improvement of the accuracy of the tests: in earlier experiments, when the analysis was not applied for finding of secondary sites, the relative error of a series exceeded 18 % .

Similar analysis, although more complicated by taking into account temperature inhomogeneities in the wave path and the temperature dependences of the Young modulus and the material density, applies to the tests in elevated temperatures, Najar at al., 1993. Here, the results for alumina in temperatures up to 1000 ^oC exhibit the same scatter as the room temperature measurements.

5 Effects of the continuum damage

The correction for non-linear material response due to the development of continuum damage prior to the fracture in spalling is based on the tensile damage model, Najar, 1987, with later improvements, s. Najar, 1993. According to it, continuum damage in ceramics develops through activation of initial damage sources, like intergranular microcracks, pores or impurities, present in the specimen since its fabrication. Due to their relatively low activation energy barrier in the tensile mode, the effects of their expansion and coalescence dominate over those of nucleation of new damage sources. Considerably higher activation stresses in compression result in the following simple model in uniaxial variable loading:

$$\sigma = E\varepsilon_{eff} \tag{1}$$

with

$$\varepsilon_{eff} = \varepsilon - \varepsilon_r \tag{2}$$

Here, the residual strain ε_r develops only in tensile loading, according to the rate rule

$$d\varepsilon_r = Dd\varepsilon + \varepsilon_{eff}dD, \qquad \varepsilon_{eff} > 0, \quad d\varepsilon > 0 \tag{3}$$

where damage D complies to the damage evolution rule in tensile loading

$$dD = \frac{E}{W^*}D\varepsilon_{eff}d\varepsilon, \qquad \varepsilon_{eff} > 0, \quad d\varepsilon > 0 \tag{4}$$

In unloading ($d\varepsilon \leq 0$), as well as in compression ($\varepsilon_{eff} < 0$), there is neither damage evolution nor change of the residual strain possible.

For initial conditions: $D = D_0$ at $\varepsilon = 0$, where D_0 is the amount of initial damage, while E denotes the Young modulus of the undamaged material and W^* represents the continuum damage energy absorptive capacity of the material, one obtains a well - posed problem for the above set of relations, unequivocally describing the non-linear response to a transient dynamic process $\varepsilon(t)$.

For monotonic tensile loading, the response of typical alumina ceramics is shown in Fig. 6. Here, a spall limit σ_{spall} can be predicted when the model's parameters E, D_0 and W^* are available.

Similarly, for a given variable loading transient process, the corresponding spall stress can be easy computed, depending though, besides the three model parameters, on the process itself, due to possible loading - unloading interactions.

Applied to the present tests, this would imply that basically there is no unique spalling stress value existent within the framework of the non-linear modelling.

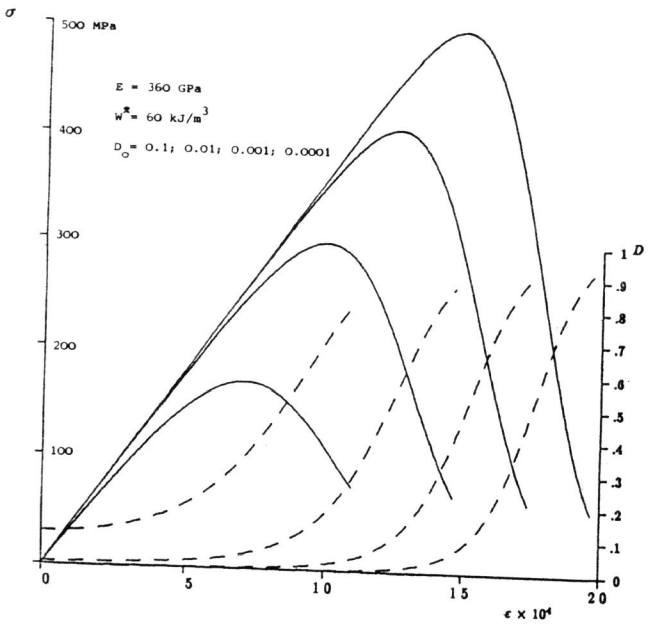

Figure 6: Stress - strain relation and damage evolution at monotonic tensile loading

Still, from a practical point of view, taking into account the variety of loading pulse shapes available in the present tests, s. Ch. 3, the range of change of the theoretical spalling strength is narrower, at least for the tested kinds of ceramics, than the scatter range of the experimental results evaluated within the linear elastic modelling, as presented above.

Therefore, the corrective procedure for material non-linearity does not have much influence on the mean strength value of an experimental series. It is related rather to the inverse problem of the determination of the unknown material characterics of the specimen by means of the dynamic test.

The evaluation of the spalling stress can be thus based on an iteration procedure, which incorporates a search subroutine for the value of the unknown initial damage D_0 of the specimen, while the other two parameters E and W^* are taken from static tests with the same kind of ceramics, assuming their strain rate independence within the rate domain of the present test.

For the reflected pulse in the specimen, the usual procedure of characteristics can be now applied, based on the knowledge of the oncoming transmitted pulse σ_t and on the condition of reflection at the stress - free end of the specimen.

The effect of the wave dispersion due to material non-linearity comes into the picture when the resultant stresses switches from the compressive into the tensile region. The incremental relations along the characteristics correspond to the stress - dependent incremental wave velocities, s. Kolsky, 1953, and are fitted into the picture obtained in the previous evaluation steps, s. Ch. 4, until the time - step sequence of the stress distributions along the specimen indicates fitting of the stress peak with one of the spalling sites determined in the test.

6 Acknowledgements

The work presented here has been performed in relation with the DFG project Na-218 on dynamic testing of high performance ceramics. Mr. S. Bierwirth has supervised the construction of the experimental arrangement and conducted the tests. The financial support of the German Research Community and Mr. S. Bierwirth's cooperation are hereby gratefully acknowledged.

References

[1] Barker,L.M., Lundergan, C.D., Herrmann, W., Dynamic response of aluminum, J. Appl. Phys.(1964), v. 35, pp. 1203-1212.

[2] Bellendir, E.N., Belyaev, V.V., Naimark, O.B., Kinetics of the multisource damage in spalling, Letters to the J. Techn. Phys. (1989), v. 15, no.13. pp. 90-93 (in Russian).

[3] Bierwirth, S., Najar, J., Versuchsanordnung zur Bestimmung der einachsigen dynamischen Zugfestigkeit elastisch-sproeder Werkstoffe, VDI Bericht 815: Experimentelle Mechanik, 13. GESA-Symposium, Bremen, 1990. VDI-Verlag, Duesseldorf (1990), pp. 403-421.

[4] Davies, R.M., A critical study of the Hopkinson pressure bar, Phil. Trans., London R. Soc., ser. A (1948), v. 240, p. 375-388.

[5] Duffy, J., Nakamura, T., Yeshurun, Y., Suresh, S., Dynamic fracture of ceramics, in: Materials at high strain rates, Int. Conf., Inst. Phys. Conf., ser. no. 102 (1989), Oxford, IOP Publ., p. 355-362.

[6] Horii H., Nemat-Nasser, S., Brittle failure in compression, Phil. Trans., London R. Soc., ser. A (1986), v. 319, p. 337.

[7] Kolsky, H., Stress waves in solids (1953), Oxford Univ. Press.

[8] Kussmaul, K., Demler, T., Klenk, A., Advanced testing method for rotating disc impact machine, in: Materials at high strain rates, Int. Conf., Inst. Phys. Conf., ser. no. 102 (1989), Oxford, IOP Publ., p.157-164.

[9] Najar, J., Continuous damage of brittle solids, in: Continuum damage mechanics, eds.: D. Krajcinovic, J. Lemaitre, Springer (1987), pp. 233-294.

[10] Najar, J., Brittle residual strain and continuum damage at variable uniaxial loading, submitted to the Int. J. Damage Mechanics (1993).

[11] Najar, J., Bierwirth, S., Einfluss der Temperatur auf die wellendynamische Zugfestigkeit und das Dispersionsverhalten von Al_2O_3-Keramik, DVM-Arbeitskreis "Bruchvorgaenge", 25. Vortragsveranstaltung, Karlsruhe, 1993, ed. D. Munz, DVM (1993).

[12] Nicholas, Th.,Tensile testing of materials at high strain rates, Exp. Mechs. (1981), v. 21, pp. 177-185.

[13] Rajendran, A.M., Cook, W., A comprehensive review of modelling of impact damage in ceramics, Rep. AFATL-TR-88-143 (1988), Univ. Dayton Res. Inst.